IEEE Access
Multidisciplinary | Rapid Review | Open Access Journal

Received January 13, 2020, accepted January 26, 2020, date of publication January 31, 2020, date of current version February 11, 2020.

Digital Object Identifier 10.1109/ACCESS.2020.2970613

Modeling and Control of Dish-Stirling Solar Thermal Integrated With PMDC Generator Optimized by Meta-Heuristic Approach

RAMESH KUMAR[1], (Member, IEEE), AND NIDUL SINHA[2], (Senior Member, IEEE)
[1]National Institute of Technology Mizoram, Aizawl 796012, India
[2]National Institute of Technology Silchar, Silchar 788010, India

Corresponding author: Ramesh Kumar (rameshelectric@gmail.com)

ABSTRACT This paper proposes an autonomous microgrid system for the first time with solar thermal dish-Stirling engine coupled with permanent magnet direct current generator and battery energy storage system along with uncontrolled variable loads. Both proportional-integral (PI) and proportional-integral-derivative (PID) controllers are considered separately for the bidirectional charge controller and buck-boost converter controller for the dish-Stirling system. The modern meta-heuristic algorithms including recent ones like particle swarm optimization, mine blast algorithm and grey wolf optimizer (GWO), have been adopted for tuning the gain parameters of the controllers used for the direct current common bus voltage stability and power sharing. The work considers variable insolation level for somehow mimicking the natural solar variation all the day. The simulation of the proposed model is carried out in MATLAB/Simulink and the results are obtained with two types of controllers for comparison. The results demonstrate the superior performance of the PID controllers optimized with GWO algorithm in terms of faster convergence rate, DC voltage profile, and maintenance of SOC of battery and energy efficiency as compared to the other two algorithms. It is also to be noted that the use of a permanent magnet DC generator coupled to the solar dish-Stirling engine improves the electric conversion efficiency and reduces cost effectively as compared to AC generators.

INDEX TERMS DC-DC converter, grey wolf optimizer, microgrid, PI/PID controller, solar dish-stirling, voltage stability.

I. INTRODUCTION

An increase in population and technology developments demand more and more energy to fulfill their energy requirements. The conventional energy sources like thermal power station and hydropower plants are not sufficient to meet the total energy requirement. The large hydropower plants affect the environment and ecosystem whereas thermal power plants emit pollutants (like CO_2, SO_2, etc.) into the air and cause the environment temperature to increase. Due to global warming, there is international pressure to reduce the CO_2 emission by shutting down the sources of these types of harmful gases. Non-conventional distributed energy sources are the solution to these problems. India has initiated to form an international solar alliance of those countries who receive sufficient solar irradiance to generate electric power to curtail carbon emission.

Dish-Stirling (DS) solar-thermal system is a prominent source of renewable energy and having recent technology for electrical power generation. Dish-Stirling solar-thermal system (DSTS) has the highest efficiency (around 30%) among all other solar-thermal power generation systems by converting direct solar irradiance into electricity considering losses [1]. Fig. 1 shows the mechanical design of DSTS in which the Stirling engine is placed at the focal point of the parabolic concave mirror or dish collector. Stirling engines are mechanical devices working on the principle of the Stirling cycle; solar receivers are so designed to transfer the received solar energy to the compressible working fluid like air, hydrogen, helium, nitrogen or even vapor [2]. The Stirling engines convert solar heat energy into mechanical power by compression and expansion of working fluid during cooling and heating of it respectively. The compression and

The associate editor coordinating the review of this manuscript and approving it for publication was Lei Yang.

This work is licensed under a Creative Commons Attribution 4.0 License. For more information, see http://creativecommons.org/licenses/by/4.0/

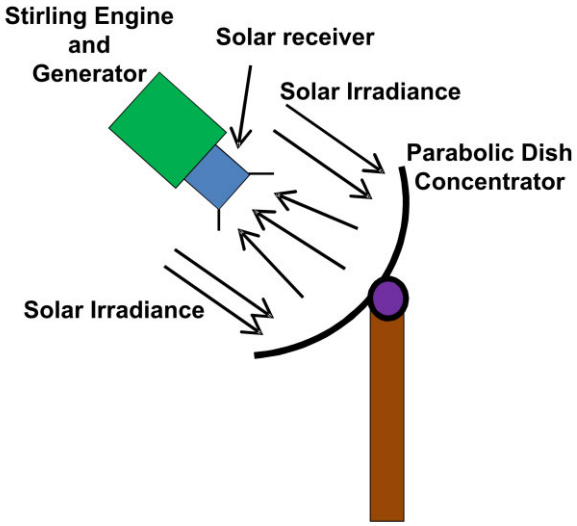

FIGURE 1. Solar dish-Stirling system.

expansion of working fluid produce linear motion which is to be converted into rotary motion and acts as a prime mover for the generator connected to it for the generation of electrical power [3], [4]. Review of the literature shows that most of the researchers have used induction generators for power generation through DSTS [5]–[9]. Whereas some of the authors adopted the permanent magnet synchronous generator (PMSG) for energy conversion purposes [10]. Control schemes of doubly fed induction generator (DFIG) and PMSG are complex and hence attract more troubles in controlling them. On the other hand, one more converter rectifier is required to get power for a DC bus system.

In the proposed work, DSTS is coupled with a Permanent Magnet Direct Current (PMDC) generator instead of AC generators, which eliminates the demand of extra converter rectifier for the DC system and enhances its efficiency [11]. The block diagram of the proposed autonomous DC microgrid system is shown in Fig. 2. DC microgrid system is directly connected to the DSTS, battery bank and the loads via DC-DC converters as shown in the figure. Most of the power demand is fulfilled by the solar DS system, whereas the battery energy storage system (BESS) stabilizes the DC bus voltage and supplies extra power demand for the time being. Voltage stability analysis has been carried out in the proposed work under a change in load demand.

Different controllers like PI and PID for the DC-DC converter switching have been considered for the purpose of comparative analysis. Manual tuning of the gain constants of these controllers is laborious and time-consuming; therefore many meta-heuristic optimization algorithms are being used for the purpose [12]–[16]. Authors in papers [12] and [13] proposed particle swarm optimization (PSO) to tune the gain parameters of PI and PID controllers respectively. Energy conversion using PMDC generator controlled by PSO based PID controller is presented in the article [14]. Paper [15] reported the grasshopper optimization algorithm for tuning the gain constants of PID controllers. Authors in paper [16] proposed genetic algorithm (GA), PSO and mine blast algorithm (MBA) to tune the gains of PID controllers, whereas in paper [17] GA and ant colony optimization are used for tuning the gain parameters of PI controllers.

The main contributions in this work are as follows:

(i) Introduced the PMDC generator with the solar dish-Stirling system for the first time for power generation with greater efficiency.

(ii) Designing the MATLAB simulation model of DSTS system with BESS for investigating the DC bus voltage stability of an autonomous microgrid system under variable solar insolation and variable loads.

(iii) Tuning the gain parameters of the controllers (PI and PID) using the meta-heuristic algorithms like PSO, MBA and GWO.

(iv) Comparative analysis of the performance of the controllers optimized with different optimization algorithms, PSO, MBA and GWO.

The paper is organized as follows: The mathematical modelling of the solar dish-Stirling system and battery energy storage system are described in section II. Section III gives complete modelling of control systems for dish-Stirling system converters and battery energy storage system. Also, the recent optimizer algorithms considered in this work are discussed in this section. Section IV presents the results obtained with the controllers and their detailed analysis. Section V brings out contributory conclusions in this work.

II. MATHEMATICAL MODELLING OF AUTONOMOUS MICROGRID

The power produced by the proposed autonomous microgrid comprising DSTS which drives the PMDC generator to produce power depends upon solar irradiance intensity. Since sufficient solar insolation is not available all the time hence BESS is connected to the DC bus through a bidirectional DC-DC converter. Uncontrolled variable resistive household loads are connected to the DC bus through uncontrolled switches (S1, S2, ...Sn) respectively as shown in Fig. 2.

A. SOLAR DISH-STIRLING ENGINE

Solar dish-Stirling engine system consists of a parabolic reflector dish and a Stirling engine. Insolation falling on the parabolic reflector compresses the working fluid to drive the Stirling engine placed at the focal point of the parabolic reflector. The compressible working fluid such as air, hydrogen, helium, nitrogen or vapour situated inside the Stirling chamber gets heated and moves to the cold space from the hot space. After getting cold the fluid moves to the hot space and hence Stirling cycle completes [3], [18]. A piston connected through the fluid chamber moves to and fro and gives linear motion due to compression and expansion of the fluid. Further, it is converted into rotational motion which is used to rotate the rotor of the generator for the generation of electric power. The concentrated solar insolation on the

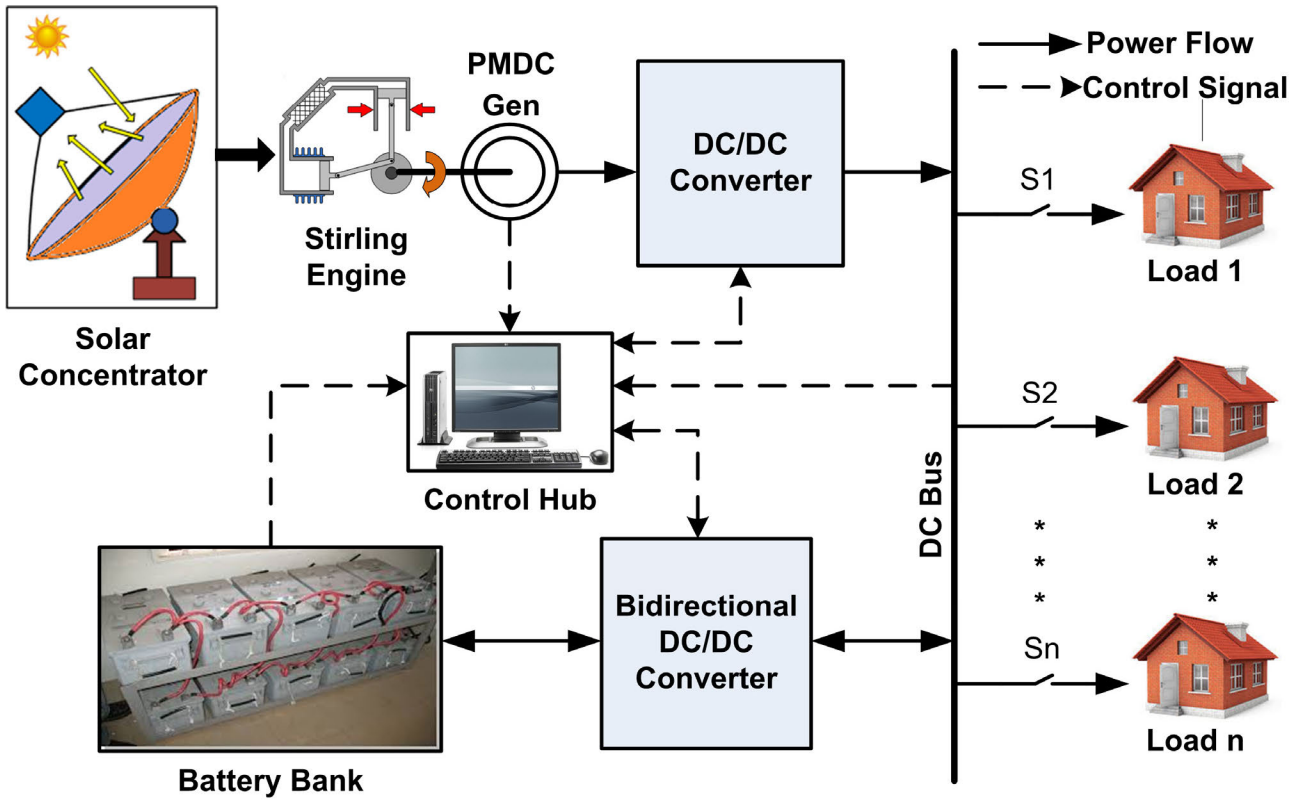

FIGURE 2. Block diagram of proposed autonomous DC microgrid system.

Stirling engine is converted into heat energy [8] as

$$Q_I = \eta_{con} A_{con} I \tag{1}$$

where η_{con} is the overall efficiency of the concentrator, A_{con} is the projected area of the parabolic type dish concentrator, and I is the irradiance level. The mechanical torque equation produced by DSTS as the input to the DFIG proposed by Thombare and Verma [19] has been modified for the application of the proposed PMDC generator in this work. The absorbed heat flow rate or useful heat energy and generated mechanical power of the Stirling engine are respectively

$$\begin{aligned} Q_h &= \eta_h Q_I \\ &= \eta_h [K_h P_{mean} \omega_m + A_h G_r + C_h P_{mean} T_h] \end{aligned} \tag{2}$$

and

$$P_m = \eta_m K_m P_{mean} \omega_m \tag{3}$$

where η_h and η_m are the efficiency coefficients of heat energy and mechanical power generated respectively, P_{mean} is the mean pressure of the working fluid and ω_m is the engine speed. K_h, A_h, K_m and C_h are the constants; G_r is the total gas flow rate and T_h is the temperature of the heat absorber. The expression of the efficiency coefficients are expressed as

$$\eta_h = \frac{\sum_{i=0}^{1} \sum_{j=0}^{1} a_{ij} P_{mean}^{i} \omega_m^{j}}{K_h P_{mean} \omega_m} \tag{4}$$

$$\eta_m = \frac{\sum_{i=0}^{1} \sum_{j=0}^{2} b_{ij} P_{mean}^{i} \omega_m^{j}}{K_m P_{mean} \omega_m} \tag{5}$$

where a_{ij} and b_{ij} are the multivariate polynomial coefficients based on the actual input and output powers of the Stirling engine respectively. The expression of the steady-state mean pressure for the working fluid to harness the maximum mechanical power is expressed as

$$P_{mean} = \frac{K_{con} I - a_{01} \omega_m - a_{00} - (1 - T_a)/K_{rec}}{a_{11} \omega_m + a_{10}} \tag{6}$$

where T_a is the normalized atmospheric temperature, K_{con} and K_{rec} are the constants and their values depend upon the thermal efficiency, projection area and thermal characteristics of the heat absorber. The expression of the mechanical torque is obtained by using equations (2), (5) and (6),i.e.

$$\tau_m = \sum_{i=0}^{1} \sum_{j=0}^{2} b_{ij} \left(\frac{K_{con} I - a_{01} \omega_m - a_{00} - (1 - T_a)/K_{rec}}{a_{11} \omega_m + a_{10}} \right)^{i} \omega_m^{j-1} \tag{7}$$

The values of the constants used in the previous equations are as follows: $A_h = -0.2735$, $C_h = 0.8752$, $K_{con} = 1.756$, $K_{rec} = 2.865$, $a_{00} = 0.045$, $a_{01} = 0.20$, $a_{10} = 0.068$, $a_{11} = 2.14$, $b_{00} = -0.038$, $b_{01} = 0.055$, $b_{10} = -0.072$, $b_{11} = 1.21$, $b_{12} = -0.13$ [19]. The mechanical torque produced is fed to the rotor shaft of the PMDC generator for the electrical

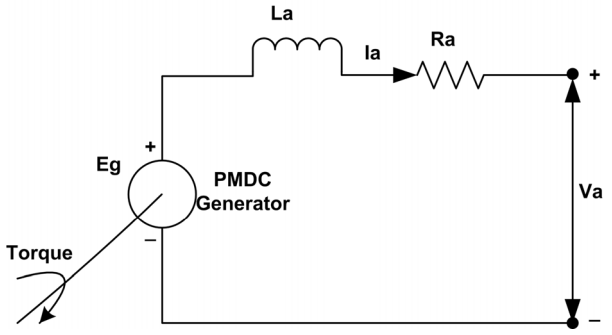

FIGURE 3. Equivalent circuit diagram of PMDC generator.

TABLE 1. PMDC generator parameter values [20].

Parameters	Values
Ra	8.5
La	5.621 mH
Kt	0.062 Nm/A
Ba	5.663×10^{-5} Nm.sec/rad
J_m	5.902 Kg.m^2
Viscous friction	5.66×10^{-5} Nm.sec/rad

power generation. The mathematical modelling of the PMDC generator has been explained in detail as below in this paper.

B. PMDC GENERATOR

The equivalent circuit diagram of the PMDC generator is illustrated in Fig. 3 [20], and the torque is provided to it by a DS engine. The generator armature coil inductance and resistance are La and Ra respectively. Voltage induced is Eg, whereas voltage available across the terminals of the generator is Va, and armature current is Ia. By applying Kirchhoff's voltage law the circuit equation obtained is

$$Va = Eg - L\frac{di}{dt} - Ra.Ia \tag{8}$$

$$Eg = Kg\omega_m \tag{9}$$

where Kg is the back emf constant, i is the instantaneous current and ω_m is the speed of the rotor shaft. The mechanical torque balance equation is expressed in equation (10).

$$\tau_m = Kt.Ia - J_m\frac{d\omega_m}{dt} - Ba.\omega_m \tag{10}$$

where Kt, Ba and J_m are torque constant, damping coefficient and moment of inertia of the machine respectively. The parameter values of the PMDC generator used are presented in Table 1.

C. BATTERY ENERGY STORAGE SYSTEM

Solar irradiance does not remain constant all the time and load is also variable in nature. In this situation, the energy balance can be ensured by introducing a battery energy storage system to the microgrid system for the DC bus voltage stability at the predefined voltage level [21]. The battery operates in charging mode during extra power generation by DSTS until the state of charge (SOC) reaches maximum predefined level and operates in discharging mode during lesser power generation than load demand until SOC reaches the minimum specified level. Charging and discharging of the BESS are controlled by the bidirectional DC-DC converter. Lithium-ion (Li-ion) type batteries have better energy density, maintenance-free and better life expectancy and hence used in the proposed work as BESS [22], [23]. The sizing of a battery depends upon the energy supply required from it [24] and the efficiency of the Li-ion battery depends on the charging and discharging rate of it [25]. If the energy requirement is E_b (kJ), then the ampere-hour (Ah) rating of the battery can be evaluated from the equation given below [26].

$$E_b = \frac{Ah \times V_{bat} \times 3600}{1000} \tag{11}$$

where V_{bat} is the voltage rating of the battery used.

The battery energy E_b is governed by the following equation [27]:

$$E_b(t) = E_b(t-1) + [P_{ds}(t)\eta_{con1} - P_L(t)]\,\eta_{con2}\eta_b^{ch} \tag{12}$$

where $E_b(t)$, $P_{ds}(t)$, $P_L(t)$ are battery energy, dish-Stirling power and load power demand at time t respectively; $E_b(t\text{-}1)$ is the battery energy at time (t-1); η_{con1}, η_{con2}, and η_b^{ch} are buck-boost converter efficiency, bidirectional converter efficiency and battery charging efficiency respectively. When the load demand is more than the power generation from DSTS the battery energy equation will be [27]

$$E_b(t) = E_b(t-1) - [P_L(t) - P_{ds}(t)\eta_{con1}]\,\eta_{con2}\eta_b^{dch} \tag{13}$$

where η_b^{dch} is the battery discharging efficiency. The values of the efficiencies are $\eta_{con1} = \eta_{con2} = 95\%$, $\eta_b^{ch} = 80\%$, and $\eta_b^{dch} = 100\%$.

D. DC-DC POWER CONVERTERS

There is more than one source of energy connected to the common DC link/bus. Therefore it is the requirement of DC-DC power converters to maintain the common DC bus voltage constant. A non-inverting buck-boost converter connects the dish-Stirling system to the common DC bus. Bidirectional DC-DC power converter connects BESS to the common DC bus. The circuit diagram of a non-invertible buck-boost converter is shown in Fig. 4 [17]. Vin is the voltage obtained from the PMDC generator and Vdc is the DC bus voltage magnitude. S1 and S2 are power electronics switches, MOSFETs are used in the proposed work. Values of the converter parameters under boost mode are obtained from the following equations [39]:

$$L > \frac{V_{in}^2(V_{dc} - V_{in})}{f_{sw}.K_{ind}.I_o.V_{dc}^2} \tag{14}$$

$$C_2 > \frac{I_o.D_{S2}}{f_{sw}.V_{dc}} \tag{15}$$

where f_{SW}, K_{ind}, D_{S2} and I_o are the switching frequency, estimated coefficient, duty cycle of switch S2 and output

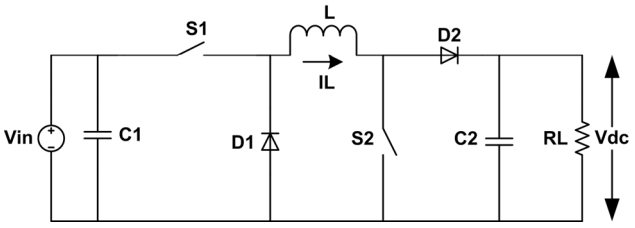

FIGURE 4. Circuit diagram of non-inverting buck-boost power converter.

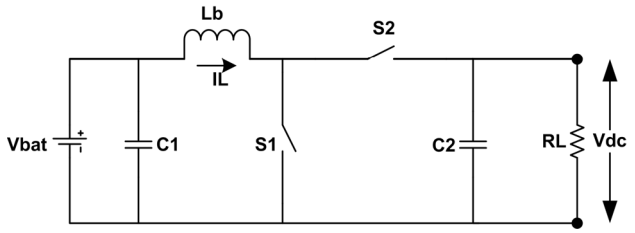

FIGURE 5. Circuit diagram of DC-DC bidirectional power converter.

current respectively. The values of the converter parameters are as follows: Vin=20 V, Vdc=60 V, $f_{SW} = 10$ kHz, $K_{ind} = 0.3$, $I_o = 30$A, C1=5 mF, C2=3 mF and L=1 mH.

The circuit diagram of a bidirectional DC-DC power converter is shown in Fig. 5. Vbat is the nominal voltage level of BESS, S1 and S2 are semiconductor switches (MOSFET for this work). During charging mode, it behaves as a buck converter and as a boost converter during the discharging mode. The design considerations of the bidirectional converter are as follows [40]:

$$L_b > \max\left[\begin{array}{l}\dfrac{V_{dc}}{\Delta I_L . f_{SW} . I_o}.D_{S1}(1-D_{S1})^2; \\ \dfrac{V_{dc}}{\Delta I_L . f_{SW} . I_o}.D_{S2}^2(1-D_{S2})\end{array}\right] \quad (16)$$

$$C_1 > \frac{1-D_{S2}}{8L_b.\Delta V_{bat}.f_{SW}^2} \quad (17)$$

$$C_2 > \frac{I_o.D_{S1}}{\Delta V_{dc}.f_{SW}} \quad (18)$$

where D_{S1} and D_{S2} are the duty cycles of switches S1 and S2 respectively. ΔI_L and ΔV_{dc} are change in inductor current and output voltage respectively. The converter parameter values for the proposed system are as follows: Vbat=24 V, Vdc=60 V, $f_{SW} = 10$ kHz, $\Delta I_L = 1.5$ A, $\Delta V_{dc} = 0.5$ V, $L_b = 0.4$ mH, C1= 5 mF, and C2=8 mF.

The power ratings of the different components used in the proposed microgrid are shown in Table 2.

III. CONTROLLER DESIGN STRATEGIES

The considered DSTS/BESS hybrid system is shown in Fig. 6; where V_{dc}^*, V_{dc}, I_{Lds}, I_{Lds}^*, I_{Lbat}, and I_{Lbat}^* are DC reference voltage, DC bus voltage, inductor current of the buck-boost converter for DSTS, inductor reference current generated for DSTS converter, inductor current of the bidirectional converter of BESS system, and inductor reference current generated for BESS bidirectional converter respectively.

TABLE 2. Power ratings of components used.

Components	Power Ratings
Dish-Stirling System	3 kW
PMDC generator	3 kW
Battery Energy Storage System	150 Ah
Buck-boost converter	3 kW
DC-DC bidirectional converter	2 kW

TABLE 3. Battery charger operating conditions.

Conditions	Mode of operation
$V_{dc} > V^*_{dc}$ & 20% ≤ SOC ≤ 90%	Charging
$V_{dc} < V^*_{dc}$ & 20% ≤ SOC ≤ 90%	Discharging
$V_{dc} = V^*_{dc}$	No operation
SOC < 20%	No discharging
SOC > 90%	No charging

A. DISH-STIRLING AND BATTERY CHARGE CONTROLLERS

The DSTS DC-DC buck-boost converter is controlled to inject the power to the DC bus, while the battery bidirectional DC-DC converter is controlled to regulate the DC bus voltage and feeds/draws extra power in the system. As per the block diagram shown in Fig. 6 (b), DC bus voltage error is fed to the PI or PID controller which generates reference current for the inner current control loop. Triangular pulse with modulation (PWM) technique is considered for the generation of firing pulses which are fed to the converter switches as per the requirement of boost mode or buck mode operation [28].

The block diagram of the DC-DC bidirectional controller is shown in Fig. 6 (c), where the switching pulses are generated like the pulses obtained for the buck-boost converter in the DSTS system. The charging and discharging mode of operations are controlled as per DC bus voltage level and SOC of the battery bank connected. The conditions of operation are given in the following Table 3:

B. OPTIMIZATION ALGORITHMS FOR AUTONOMOUS MICROGRID SYSTEM

Many heuristic algorithms have been developed for getting the optimum solution for complex optimization problems. Optimization may be a minimization or maximization problem. In the proposed work minimization of voltage deviation is considered as the objective for the purpose of evaluating the performance of the PI/PID controllers used. The authors have adopted integral absolute error (IAE) of voltage deviation ΔV

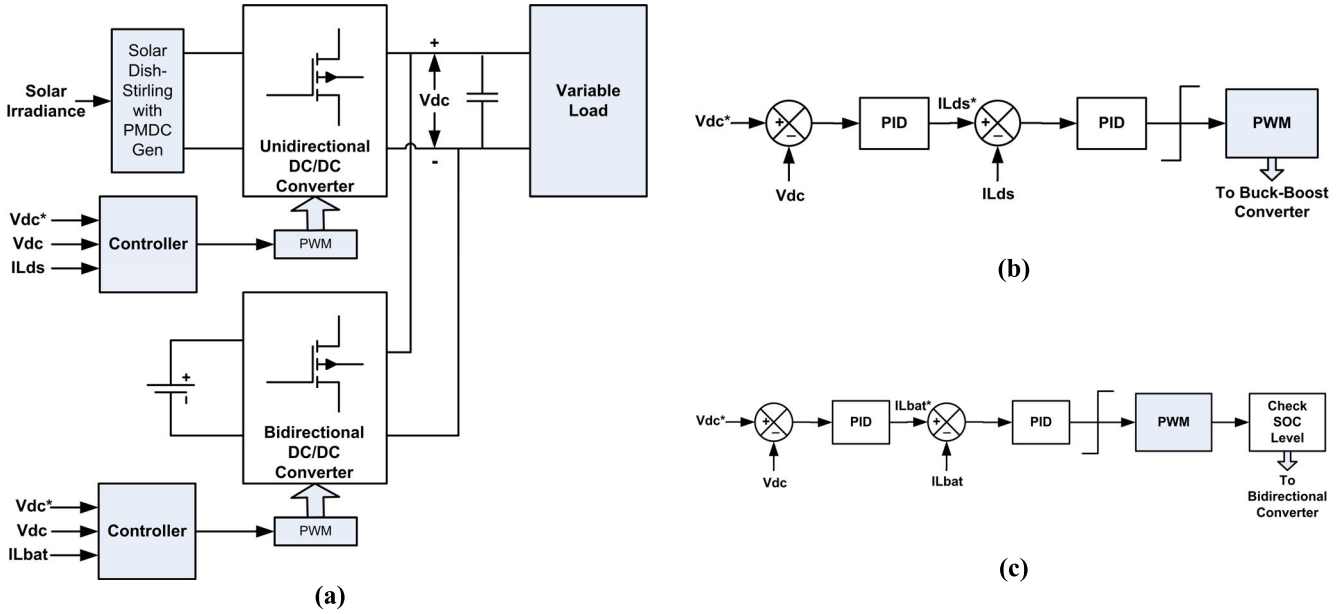

FIGURE 6. (a) Block/Circuit diagram of proposed microgrid system, (b) Control loop of DSTS, and (c) Control loop of BESS.

TABLE 4. Boundary conditions of gain constants.

Controller type	Boundary conditions
PI	$K_P^{\min} \le K_P \le K_P^{\max}$
	$K_I^{\min} \le K_I \le K_I^{\max}$
PID	$K_P^{\min} \le K_P \le K_P^{\max}$
	$K_I^{\min} \le K_I \le K_I^{\max}$
	$K_D^{\min} \le K_D \le K_D^{\max}$

as an objective function J as shown in equation (19)

$$J = \int_0^t |\Delta V| dt = \int_0^t \left|\left(V_{dc}^* - V_{dc}\right)\right| dt \tag{19}$$

The boundary conditions of the gain constants are shown in Table 4.

Meta-heuristic optimization algorithms have become popular for the last few years and are being applied for optimizing the gain parameters of the PI and PID controllers. Some of them are like genetic algorithm (GA) proposed by Holland [29] in 1975 and Goldberg [30] in 1989, ant colony optimization (ACO) is proposed by Dorego in 1992, particle swarm optimization (PSO) proposed by Kennedy and Eberhart [31] in 1995, artificial bee colony (ABC) proposed by Karaboga in 2005, cuckoo search algorithm proposed by Yang and Dev in 2009, bat algorithm proposed by Yang in 2010, flower pollination algorithm proposed by Yan in 2012, etc. Recent algorithms such as mine blast algorithm (MBA) and grey wolf optimizer (GWO) have been proposed for optimizing the gain parameters of PI/PID controllers for automatic generation control and reported to give impressive results as compared to most popularly used PSO.

PSO is inspired by the behavior of birds flock or swarm in search of food. The values of acceleration constants c_1 and c_2 are considered 2.0 in this case whereas inertia weight is taken less than 0.7. The main steps of PSO algorithms are as follows [32]:

Step 1: Initialization of a population of particles.

Step 2: Find the fitness value for each particle.

Step 3: Compare the fitness value of each particle's P-best and updates its value.

Step 3: Compare fitness with overall previous best and update global best (g-best).

Step 4: Modify the velocity and position of particles.

Step 5: Go to step 2 until convergence criteria is satisfied.

Many more literatures have explained the PSO technique; hence, it is not explained in detail in this paper. However, the other two recent algorithms, MBA and GWO have been explained in detail.

1) MINE BLAST ALGORITHM (MBA)

It is proposed by A. Sadollah et.al. in 2012 and inspired by a mine bomb explosion in which thrown pieces of shrapnel collide with other bombs and cause more explosions [33], [34]. The casualties resulted from the explosion of a mine bomb are considered as a fitness of the objective function of the mine's bomb at a location. The first shot point or initial population is created as given:

$$X_0 = LB + rand \times (UB - LB) \tag{20}$$

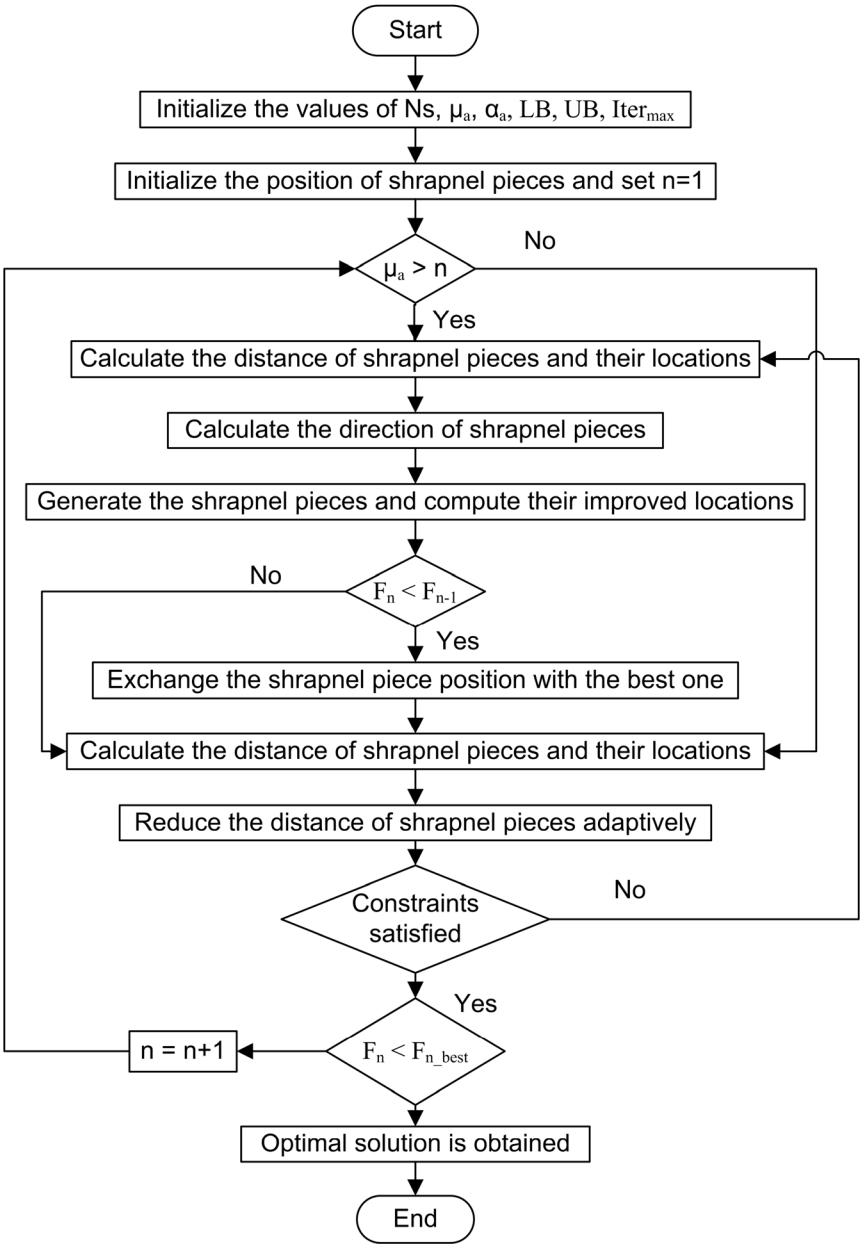

FIGURE 7. Flow chart of Mine Blast Algorithm [35].

where X_0, LB, UB and rand are initial population, lower and upper bounds of the PI/PID gain parameters and a uniform random number between 0 and 1 respectively. The current location X_n of a mine bomb at the n^{th} iteration is given as:

$$X_n = \{X_m\}; \quad m = 1, 2, 3, \ldots N_d \tag{21}$$

where N_d is the number of variables or number of gain parameters is to be optimized in this case. It is considered that N_s shrapnel pieces are created causing another mine explosion at location X_{n+1}.

$$X_{n+1} = \Delta X + \exp\left(-\sqrt{\frac{m_{n+1}}{d_{n+1}}}\right) X_n \tag{22}$$

where ΔX indicates the change in position of a shrapnel, m_{n+1} is the direction (slope) of shrapnel pieces from original explosion and d_{n+1} is distance of shrapnel pieces from original explosion. The ΔX is defined as

$$\Delta X_{n+1} = d_n \times rand \times \cos(\theta) \tag{23}$$

where θ is the angle of shrapnel pieces goes after explosion for uniform search in the domain space and can be calculated as given;

$$\theta = \frac{360^{\circ}}{N_s} \tag{24}$$

where N_s is the number of shrapnel pieces.

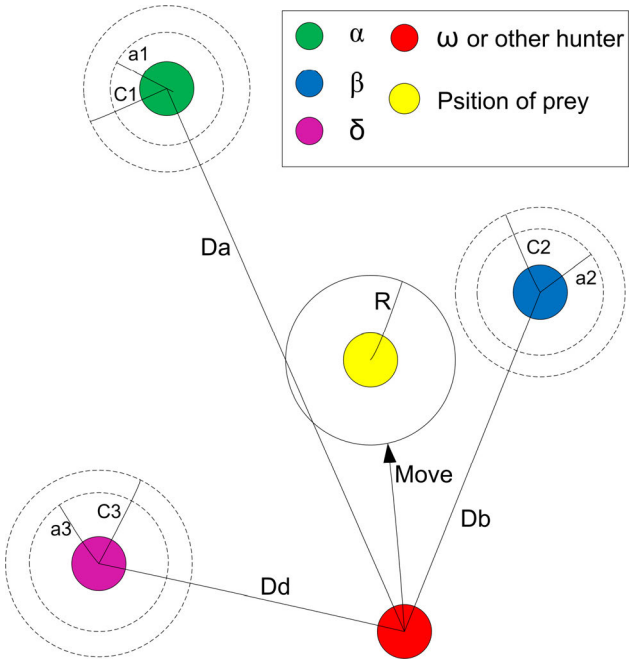

FIGURE 8. Position updating in GWO [34].

Further distance and direction are defined as

$$d_{n+1} = \sqrt{(X_{n+1} - X_n)^2 + (F_{n+1} - F_n)^2} \quad (25)$$

$$m_{n+1} = \frac{F_{n+1} - F_n}{X_{n+1} - X_n} \quad (26)$$

where F is the fitness function values of location X. The equations for the exploration in the solution space are given as:

$$d_{n+1} = d_n + (|rand|)^2 \quad (27)$$

$$\Delta X_{n+1} = d_{n+1} \times \cos(\theta) \quad (28)$$

The exploration factor μ_a provides the ability to the shrapnel pieces for the fast convergence towards the optimal point. During the exploration period equations (23) and (25) should be replaced by equations (27) and (28). As the distance traveled by shrapnel pieces is reduced, global minima is achieved and hence gives the faster convergence.

$$d_{n+1} = \frac{d_n}{\exp(k/\alpha_a)} \quad (29)$$

where α_a and k are the reduction factor and iteration number index respectively. The flow chart of the MBA optimizing the gain parameters of PI/PID controller is shown in Fig. 7 and the main steps of the algorithm are as follows:

Step 1: Initialize the values of N_s, μ_a, α_a, maximum number of iterations, LB and UB of the gain constant variables.

Step 2: Calculate the first shot point and direction of shrapnel pieces.

Step 3: Compute the next improved location of the shrapnel pieces and save the best location.

Step 4: Check the convergence criteria, if satisfied terminate the process and save all values, otherwise go to step 2.

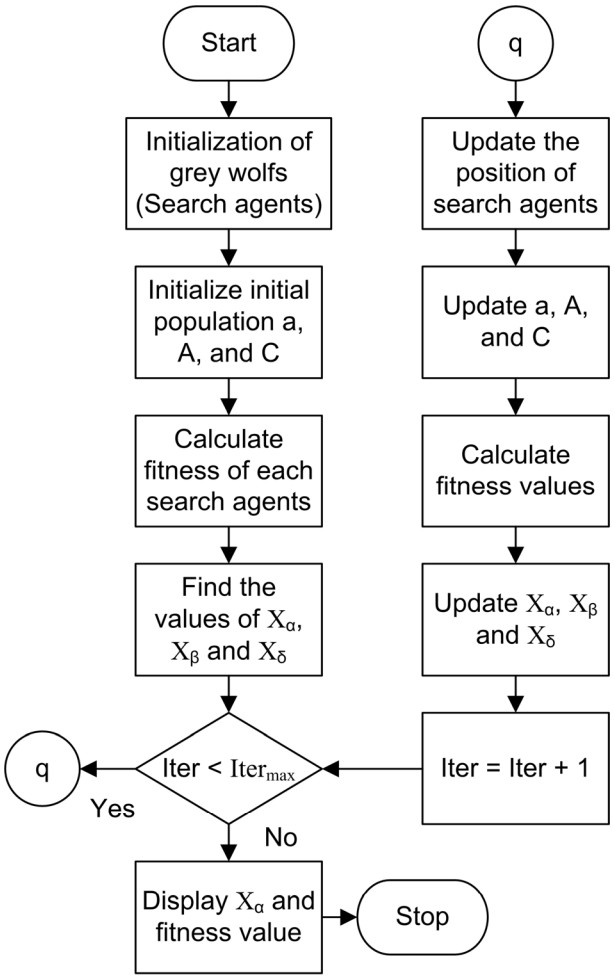

FIGURE 9. Flow chart of grey wolf optimizer.

2) GREY WOLF OPTIMIZER (GWO)

It is proposed by Seyedali Mirjalili et. al. in 2014 and it is inspired by the hunting behavior of grey wolves. The wolves in a group are divided into four categories in the wolf hierarchy as alpha (α), beta (β), delta (δ) and omega (ω). Alpha is the leader of a group and is the fittest or optimized solution of a problem. Beta wolves help alpha wolf in decision making and implementation of decisions in a group, they come in the second level of grey wolf hierarchy and they are close to optimized solution after alpha solution. Omega wolves come in the lowest ranking in a group and follow other wolves. However, delta wolves come higher ranking than omega but subordinate of alpha and beta wolves [36]. The important phases of grey wolf hunting are as follows [37], [38]:

- Searching, chasing and approaching the prey.
- Encircling and harassing the prey until it stops moving by getting tired.
- Attacking the prey.

Encircling behaviour is expressed through the following equations:

$$D = |CX_P(n) - X(n)| \quad (30)$$

TABLE 5. Optimized controller gains and minimum objective function values.

Type of Controller	J_{min} & Gain Parameters	PSO	MBA	GWO
PI	J_{min}	0.4795	0.3462	0.3459
	K_{P1}	5.0000	3.5256	3.4249
	K_{I1}	14.5691	9.7477	8.918
	K_{P2}	5.0000	7.5994	6.4511
	K_{I2}	0.0010	2.5264	1.2897
	K_{P3}	1.2853	3.9048	3.7947
	K_{I3}	226.0304	9.5613	10.0000
	K_{P4}	5.0000	9.9974	9.7983
	K_{I4}	4.1596	10.0000	3.2256
PID	J_{min}	0.8124	0.3146	0.3015
	K_{P1}	0.0010	0.0019	0.3640
	K_{I1}	11.1969	0.6379	3.4740
	K_{D1}	0.0010	0.0010	3.6861
	K_{P2}	0.0010	0.2623	1.0256
	K_{I2}	176.1293	1.18096	4.7275
	K_{D2}	1.0000	0.1876	4.0901
	K_{P3}	0.0010	0.0010	0.0017
	K_{I3}	155.3146	1.9955	10.0000
	K_{D3}	0.6976	0.0010	0.0010
	K_{P4}	1.1167	1.1167	0.0519
	K_{I4}	88.2485	0.95064	3.4777
	K_{D4}	0.0010	1.4598	2.1162

$$X\,(n+1) = X_P\,(n) - A.D \tag{31}$$

where n is the current iteration, A and C are coefficient vectors, X_P is the position vector of prey and X is the position vector of a grey wolf. A and C are calculated through the following equations:

$$A = 2a.r_1 - a \tag{32}$$

$$C = 2r_2 \tag{33}$$

where magnitude of vector 'a' decreases linearly from 2 to 0 over the course of iteration; r_1, r_2 are the random vectors whose values fall in between 0 and 1.

During the hunting process best positions of α, β and δ are saved first then the position of ω is updated as shown in Fig. 8 and given in the following equations:

$$\begin{aligned} D_\alpha &= |C_1.X_\alpha - X| \\ D_\beta &= |C_2.X_\beta - X| \\ D_\delta &= |C_3.X_\delta - X| \end{aligned} \tag{34}$$

$$\begin{aligned} X_1 &= X_\alpha - A_1.D_\alpha \\ X_2 &= X_\beta - A_2.D_\beta \\ X_3 &= X_\delta - A_3.D_\delta \end{aligned} \tag{35}$$

$$X\,(n+1) = \frac{X_1 + X_2 + X_3}{3} \tag{36}$$

Algorithm of the GWO optimizing the gain parameters of PI/PID controller are expressed through the following steps:

TABLE 6. Constant parameters of optimization techniques used.

PSO	MBA	GWO
$C_1 = 2.0$	$\mu_a = 20$	$r_1 = \text{rand}(0,1)$
$C_2 = 2.0$	$\alpha_a = 149.7007$	$r_2 = \text{rand}(0,1)$
Inertia weight < 0.7		$0 \le a \le 2$

Step 1: Initialize the initial population, a, A, C and lower and upper bounds of the gain parameters of PI/PID controllers.

Step 2: Calculation of the fitness of each search agent X_α, X_β and X_δ.

Step 3: Update the current position of search agent X_ω.

Step 4: Update the values of a, A and C.

Step 5: Calculate the fitness of each search agent and update them.

Step 6: If maximum iteration is achieved return the best solution X_α.

The flow chart of the GWO for optimizing the gain parameters of PI and PID controllers is shown in Fig. 9.

The population size and the maximum number of iterations for all the algorithms applied in this work are taken as 10 and 50 respectively. Other constant parameters of the algorithms are presented in Table 6.

IV. RESULTS AND DISCUSSION

It is shown in Fig. 6 that two PI or PID controllers are connected for the inner current control loop and the outer

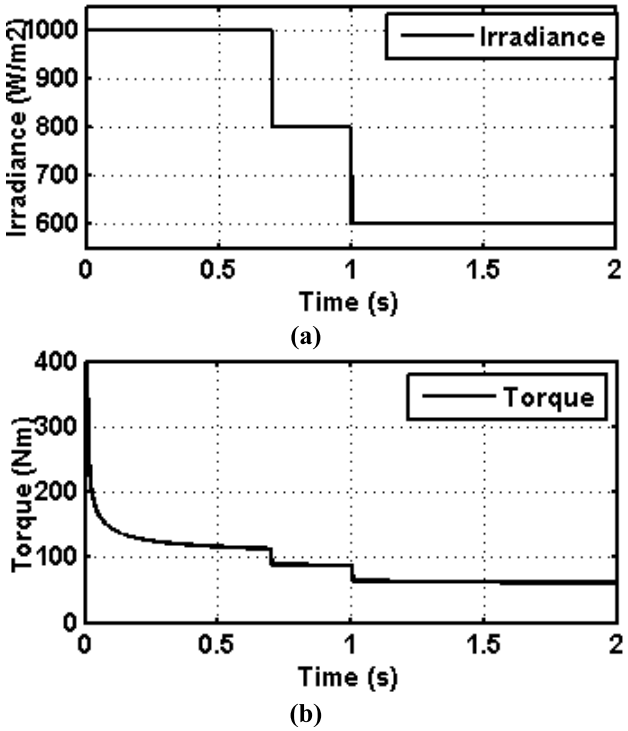

FIGURE 10. Dish-Stirling behavior on solar irradiance: (a) Variation of solar irradiance, (b) Torque produced by DSTS.

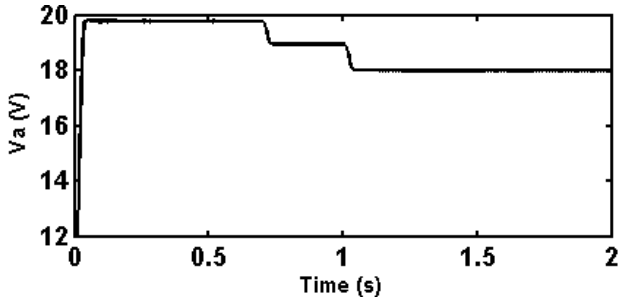

FIGURE 11. Output voltage of PMDC generator coupled with DSTS.

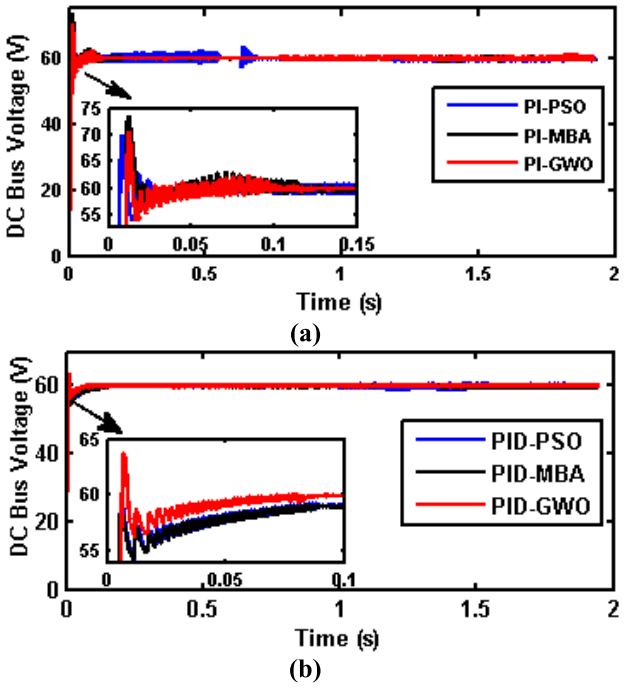

FIGURE 12. DC bus voltage curves: (a) DC bus voltage using PI controller, (b) DC bus voltage using PID controller.

voltage control loop for each converter controllers, hence total four PI or PID controllers have been used in the proposed microgrid control system. Tuning of the gain parameters of these controllers is a challenging task. Therefore, three meta-heuristic optimization algorithms, such as PSO, MBA and GWO are used separately linking with the Simulink model for PI and PID controllers separately and optimal gain constants are obtained which are presented in Table 5. The optimal values of the objective function are also listed in the table.

Solar insolation is random in nature and there is daily, monthly and yearly variation. Therefore variable irradiance input to the DSTS has been considered for this work. The irradiance changes from 1000 W/m^2 to 800 W/m^2 at 0.7 second and another change from 800 W/m^2 to 600 W/m^2 is at 1 second as shown in Fig. 10 (a). Dish-Stirling system is a thermo-mechanical device that produces mechanical torque as per equation (7) on the incidence of solar irradiance at its parabolic dish collector. The mechanical torque produced due to the irradiance as per Fig. 10 (a) is shown in Fig. 10 (b). By seeing the torque curve it is found that torque decreases as the solar insolation decreases at time 0.7 and 1 second respectively. The DSTS is mechanically coupled to the PMDC generator shaft. Therefore the variation of solar irradiance consequently there is variation in torque produced by DSTS causes the variation of the voltage induced by PMDC generator Va as shown in Fig. 11.

The mechanical torque is fed to the prime mover of the proposed PMDC generator for electrical power generation. The concept of coupling a PMDC generator with the dish-Stirling system is for the first time. This combination is not only energy efficient but also cost-efficient because the number of converters required is less in comparison to the application of AC generators. BESS is also coupled at the common DC bus through a bidirectional DC-DC converter and it is responsible for balancing surplus power, overload demand and the DC bus voltage regulation. The curves of DC bus vs. time have been obtained in both the cases of PI and PID controllers. In both the cases the Simulink model has been run with the algorithms PSO, MBA and GWO separately. The analysis of the curves shown in Fig. 12 (a) shows that there is an oscillation in the beginning stage of the DC bus voltage in case of application of PSO whereas oscillations are reduced when MBA and GWO are used for optimization. By observing Fig. 12 (b) it is evident that there is a small overshoot of DC bus voltage in the beginning. It is seen clearly in Fig. 13 that voltage overshoot with the PID controller is lesser compared to the PI controller when their gain parameters are optimized with GWO. Hence, the overall

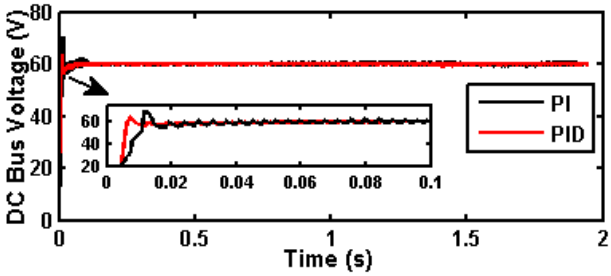

FIGURE 13. DC bus voltage using PI and PID controller optimized with GWO.

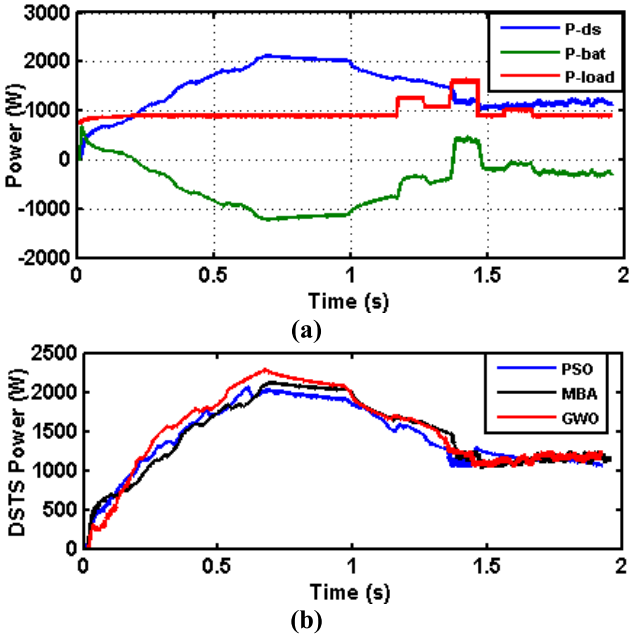

FIGURE 14. Power outputs using PID controller: (a) Dish-Stirling, battery and load power, (b) Power supplied by dish-Stirling system.

performance of the PID controller optimized with GWO in maintaining the DC bus voltage profile is better than any of the other two algorithms, PSO and MBA.

The power control and power sharing in the autonomous microgrid is shown in Fig. 14 (a). The figure shows the load power variation, DSTS power generation variation and battery power exchange. It is seen from the curve that initial load power demand is 900 watts and it is increased to more than 1500 watts as peak demand at a later stage. The power generation by DSTS increases slowly due to the dynamic behavior of the dish-Stirling system and the PMDC generator. Power generation from DSTS decrease after 0.7 seconds and again after 1 second as the irradiance level decreases making it lesser than the load demand. If the battery power curve is seen, it can be observed that initially, the battery is supplying the load power, and gradually decreasing as DSTS power generation increases. At the latter time when load power demand increases the power from the battery fulfills the extra load power demand during peak demand time. The negative battery power flow shows power flow towards the battery

TABLE 7. Convergence time of three optimization approaches represented in seconds (Sec).

Controller	PSO (Sec)	MBA (Sec)	GWO (Sec)
PI	5334.23	8055.37	5519.86
PID	6351.35	7920.12	5100.79

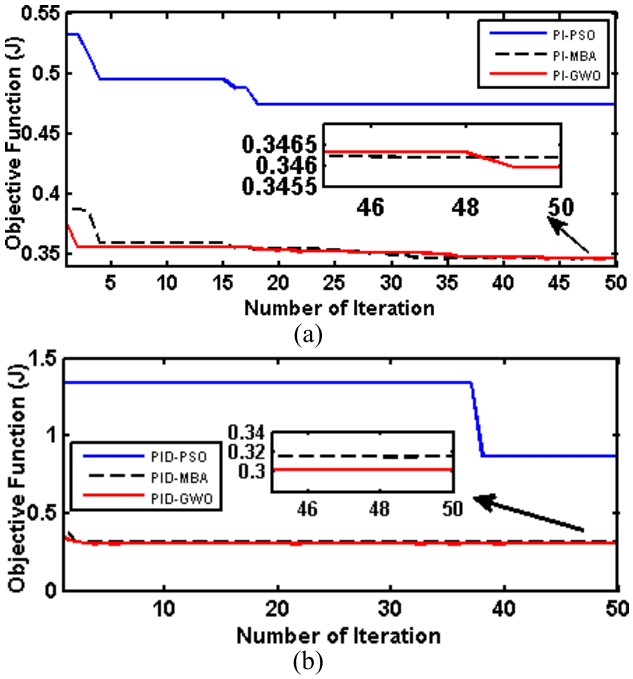

FIGURE 15. Convergence curves: (a) Using PI controller, (b) Using PID controller.

storage system as in charging operation. Fig. 14 (b) shows the DSTS power generation curves obtained by applying the three optimization algorithms. The analysis of these curves expresses that the power generation from the DSTS is more in the case of GWO algorithm as compared to the other two optimizers. That is, the power conversion efficiency is more by using optimal gain constants of PID controller obtained with GWO algorithm.

The gain optimizer algorithms have been run for maximum number of iterations as 50 and population size has been taken as 10 decided after some trial runs. The IAE is considered as an objective function (J) as per equation (17) and its optimum values are depicted in Table 5. The convergence curves of the objective function over 50 iterations are shown in Fig. 15. The figure Fig. 15 (a) shows the convergence of J in the case of PI controller obtained by applying all the three optimizer algorithms, whereas Fig. 15 (b) shows for the case of PID controller. It is found that the GWO shows a better convergence rate and gives the minimum objective function value as compared to PSO and MBA. However, in between PSO and MBA the performance of MBA is far better than PSO on the proposed microgrid model. The MATLAB simulation model of the autonomous DC microgrid system has been run in the computer having intel core i5 processor and 4GB RAM takes

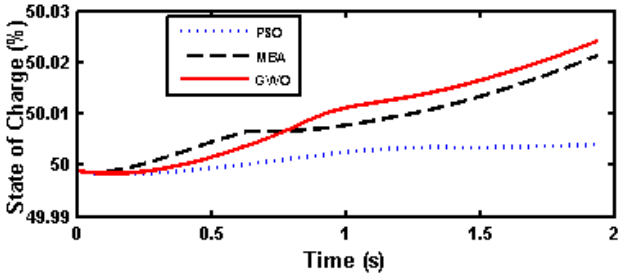

FIGURE 16. Variation of state of charge of BESS.

the convergence time by application of three optimization approaches PSO, MBA and GWO are shown in Table 7.

As Fig. 14 (a) shows that the power flows in the battery storage is bidirectional. It means that the battery operates both in charging and discharging modes as per requirements. Initially, the SOC of the battery storage is taken as 50%. Charging the battery above 90% and discharging below 20% is not good for battery health. Therefore, battery operation is considered in between 20% and 90% SOC. The SOC curves are shown in Fig. 16 for three different optimizer applications in the case of PID controller. The figure shows that the battery is getting discharged in the beginning and getting charged later on. The charging slows down and SOC remains constant or decreases during a part of the load power supply at the peak load demand. It increases after the peak demand. It is also seen that the SOC level is better with the application of GWO as compared to the other two optimization algorithms.

V. CONCLUSION

This paper proposes for the first time the coupling of PMDC generator with the dish-Stirling system instead of AC generators as reported by other researchers. The DC generator in the autonomous DC microgrid system works as a cost and energy-efficient option in an effective manner. Recent metaheuristic optimization algorithms MBA and GWO including PSO have been proposed for tuning the gain parameters of the PI and PID controllers in this proposed work. Among these three optimization algorithms, GWO shows better performance in this problem in terms of convergence rate, DC bus voltage profile, maintenance of SOC level of the battery and better energy conversion efficiency as compared to the other two algorithms, PSO and MBA. Further, power sharing between DSTS and BESS has been shown clearly during peak and normal loading conditions. It is verified through the MATLAB simulation results that the voltage stability achieved with GWO optimized PID controller under variable solar insolation and load perturbations is the best amongst the three algorithms. Future work may be carried out by considering the temperature variations of the dish-Stirling system.

ACKNOWLEDGMENT

The authors would like to thank the Department of Electrical Engineering, NIT Silchar, for providing lab and other facilities to complete this work.

REFERENCES

[1] T. Mancini, P. Heller, B. Butler, B. Osborn, W. Schiel, V. Goldberg, R. Buck, R. Diver, C. Andraka, and J. Moreno, "Dish-Stirling systems: An overview of development and status," *J. Solar Energy Eng.*, vol. 125, no. 2, pp. 135–151, May 2003.

[2] A. Hafez, A. Soliman, K. El-Metwally, and I. Ismail, "Solar parabolic dish Stirling engine system design, simulation, and thermal analysis," *Energy Convers. Manage.*, vol. 126, pp. 60–75, Oct. 2016.

[3] B. Kongtragool and S. Wongwises, "A review of solar-powered Stirling engines and low temperature differential Stirling engines," *Renew. Sustain. Energy Rev.*, vol. 7, no. 2, pp. 131–154, Apr. 2003.

[4] M. Abbas, B. Boumeddane, N. Said, and A. Chikouche, "Dish Stirling technology: A 100 MW solar power plant using hydrogen for Algeria," *Int. J. Hydrogen Energy*, vol. 36, no. 7, pp. 4305–4314, Apr. 2011.

[5] R. Pena, J. Clare, and G. Asher, "Doubly fed induction generator using back-to-back PWM converters and its application to variable-speed wind-energy generation," *IEE Proc.—Electr. Power Appl.*, vol. 143, no. 3, pp. 231–241, 1996.

[6] D. Howard and R. G. Harley, "Modeling of dish-Stirling solar thermal power generation," in *Proc. IEEE Power Energy Soc., Gen. Meeting*, Providence, RI, USA, Jul. 2010, pp. 1–7.

[7] D. Santos-Martin, J. Alonso-Martinez, J. Eloy-Garcia, and S. Arnalte, "Solar dish-Stirling system optimisation with a doubly fed induction generator," *IET Renew. Power Gener.*, vol. 6, no. 4, pp. 276–288, 2012.

[8] Y. Li, S. S. Choi, and C. Yang, "Dish-Stirling solar power plants: Modeling, analysis, and control of receiver temperature," *IEEE Trans. Sustain. Energy*, vol. 5, no. 2, pp. 398–407, Apr. 2014.

[9] Y. Kadri and H. H. Abdallah, "Performance evaluation of a stand-alone solar dish Stirling system for power generation suitable for off-grid rural electrification," *Energy Convers. Manage.*, vol. 129, pp. 140–156, Dec. 2016.

[10] G. Barreto and P. Canhoto, "Modelling of a Stirling engine with parabolic dish for thermal to electric conversion of solar energy," *Energy Convers. Manage.*, vol. 132, pp. 119–135, Jan. 2017.

[11] R. K. Chauhan, B. S. Rajpurohit, R. E. Hebner, S. N. Singh, and F. M. Gonzalez-Longatt, "Voltage standardization of DC distribution system for residential buildings," *J. Clean Energy Technol.*, vol. 4, no. 3, pp. 167–172, 2015.

[12] I.-Y. Chung, W. Liu, D. A. Cartes, and S.-I. Moon, "Control parameter optimization for multiple distributed generators in a microgrid using particle swarm optimization," *Eur. Trans. Electr. Power*, vol. 21, no. 2, pp. 1200–1216, Mar. 2011.

[13] Z.-L. Gaing, "A particle swarm optimization approach for optimum design of PID controller in AVR system," *IEEE Trans. Energy Convers.*, vol. 19, no. 2, pp. 384–391, Jun. 2004.

[14] I. Atacak and B. Kucuk, "PSO-based PID controller design for an energy conversion system using compressed air," *Technicki Vjesnik-Tech. Gazette*, vol. 24, no. 3, pp. 671–679, Jan. 2017.

[15] A. K. Barik and D. C. Das, "Expeditious frequency control of solar photovoltaic/biogas/biodiesel generator based isolated renewable microgrid using grasshopper optimisation algorithm," *IET Renew. Power Gener.*, vol. 12, no. 14, pp. 1659–1667, Oct. 2018.

[16] S. Ranjan, D. Chandra Das, S. Behera, and N. Sinha, "Parabolic trough solar–thermal–wind–diesel isolated hybrid power system: Active power/frequency control analysis," *IET Renew. Power Gener.*, vol. 12, no. 16, pp. 1893–1903, Dec. 2018.

[17] A. M. Bozorgi, V. Fereshtehpoor, M. Monfared, and N. Namjoo, "Controller design using ant colony algorithm for a non-inverting buck–boost chopper based on a detailed average model," *Electric Power Compon. Syst.*, vol. 43, no. 2, pp. 177–188, Jan. 2015.

[18] D. Thombare and S. Verma, "Technological development in the Stirling cycle engines," *Renew. Sustain. Energy Rev.*, vol. 12, no. 1, pp. 1–38, Jan. 2008.

[19] Y. Li, S. S. Choi, C. Yang, and F. Wei, "Design of variable-speed dish-Stirling solar–thermal power plant for maximum energy harness," *IEEE Trans. Energy Convers.*, vol. 30, no. 1, pp. 394–403, Mar. 2015.

[20] Z. M. Tun and T. L. Naing, "Double loop control of H-bridge DC chopper fed permanent magnet DC motor drives using low cost hardware," *Int. J. Elect. Comput. Eng.*, vol. 12, no. 11, pp. 857–866, Dec. 2018.

[21] C. A. Hill, M. C. Such, D. Chen, J. Gonzalez, and W. M. Grady, "Battery energy storage for enabling integration of distributed solar power generation," *IEEE Trans. Smart Grid*, vol. 3, no. 2, pp. 850–857, Jun. 2012.

[22] T. Mesbahi, N. Rizoug, F. Khenfri, P. Bartholomeüs, and P. Le Moigne, "Dynamical modelling and emulation of Li-ion batteries–supercapacitors hybrid power supply for electric vehicle applications," *IET Electr. Syst. Transp.*, vol. 7, no. 2, pp. 161–169, Jun. 2017.
[23] X. Huang and B. Jiang, "Research on lithium battery energy storage system in wind power," in *Proc. Int. Conf. Electr. Control Eng.*, Yichang, China, Sep. 2011, pp. 1200–1203.
[24] M. Kermadi and E. M. Berkouk, "A maximum power point tracker based on particle swarm optimization for PV-battery energy system under partial shading conditions," in *Proc. 3rd Int. Conf. Control, Eng. Inf. Technol. (CEIT)*, May 2015, pp. 1–6.
[25] P. Ariyaratna, K. M. Muttaqi, and D. Sutanto, "A novel control strategy to mitigate slow and fast fluctuations of the voltage profile at common coupling Point of rooftop solar PV unit with an integrated hybrid energy storage system," *J. Energy Storage*, vol. 20, pp. 409–417, Dec. 2018.
[26] S. Farhad and A. Nazari, "Introducing the energy efficiency map of lithium-ion batteries," *Int. J. Energy Res.*, vol. 43, no. 2, pp. 931–944, Feb. 2019.
[27] A. M. Abdelshafy, H. Hassan, and J. Jurasz, "Optimal design of a grid-connected desalination plant powered by renewable energy resources using a hybrid PSO–GWO approach," *Energy Convers. Manage.*, vol. 173, pp. 331–347, Oct. 2018.
[28] T. V. Thang, A. Ahmed, C.-I. Kim, and J.-H. Park, "Flexible system architecture of stand-alone PV power generation with energy storage device," *IEEE Trans. Energy Convers.*, vol. 30, no. 4, pp. 1386–1396, Dec. 2015.
[29] J. H. Holland, *Adaptation in Natural and Artificial Systems*. Ann Arbor, MI, USA: Univ. Michigan Press, 1975.
[30] D. E. Goldberg, *Genetic Algorithms in Search Optimization and Machine Learning*. Reading, MA, USA: Addison-Wesley, 1989.
[31] J. Kennedy and R. Eberhart, "Particle Swarm Optimization," in *Proc. Int. Conf. Neural Netw.*, 1995, pp. 1942–1948.
[32] Y. B. Xiaogang and Y. Li, "A novel particle swarm optimization algorithm," in *Proc. CCTAE*, Chengdu, China, 2010, pp. 408–411.
[33] A. Sadollah, A. Bahreininejad, H. Eskandar, and M. Hamdi, "Mine blast algorithm: A new population based algorithm for solving constrained engineering optimization problems," *Appl. Soft Comput.*, vol. 13, no. 5, pp. 2592–2612, May 2013.
[34] S. Majumdar, K. Mandal, and N. Chakraborty, "Performance study of Mine Blast Algorithm for automatic voltage regulator tuning," in *Proc. Annu. IEEE India Conf. (INDICON)*, Pune, India, Dec. 2014, pp. 1–6.
[35] A. Fathy, "A reliable methodology based on mine blast optimization algorithm for optimal sizing of hybrid PV-wind-FC system for remote area in Egypt," *Renew. Energy*, vol. 95, pp. 367–380, Sep. 2016.
[36] S. Mirjalili, S. M. Mirjalili, and A. Lewis, "Grey wolf optimizer," *Adv. Eng. Softw.*, vol. 69, pp. 46–61, Mar. 2014.
[37] C. Muro, R. Escobedo, L. Spector, and R. Coppinger, "Wolf-pack (Canis lupus) hunting strategies emerge from simple rules in computational simulations," *Behavioural Processes*, vol. 88, no. 3, pp. 192–197, Nov. 2011.
[38] A. Y. Kishore, P. V. N. Babu, J. Chinnaraj, and E. M. Raghava, "Load frequency control in deregulated power system by grey-wolf optimization algorithm," *Int. J. Control Autom.*, vol. 11, no. 8, pp. 11–24, Aug. 2018.
[39] M. Green, "Design calculations for buck-boost converters," in *Application Report, Texas Instruments*. Dallas, TX, USA: Texas Instruments, Sep. 2012, pp. 1–11.
[40] R. M. Schupbach and J. C. Balda, "35 KW ultracapacitor unit for power management of hybrid electric vehicles: Bidirectional DC-DC converter design," in *Proc. Int. Conf. IEEE Power Electron. Spec.*, Aachen, Germany, Jun. 2004, pp. 2157–2163.

RAMESH KUMAR (Member, IEEE) received the B.Tech. degree in electrical and electronics engineering from the Cochin University of Science and Technology, Kerala, India, in 2009, and the M.Tech. degree in power and energy system engineering from the National Institute of Technology Silchar, Assam, India, in 2012, where he is currently pursuing the Ph.D. degree in electrical engineering. He is currently an Assistant Professor of electrical and electronics engineering with the National Institute of Technology Mizoram, Aizawl, India. His research interests include microgrid, power quality, renewable power generation, and power management. He is also a Life Member of IE(I).

NIDUL SINHA (Senior Member, IEEE) was born in Tripura, India, in 1962. He received the B.E. degree in electrical engineering from Calcutta University, Kolkata, India, in 1984, the M.Tech. degree in power apparatus and systems from IIT Delhi, New Delhi, in 1989, and the Ph.D. degree in electrical engineering from Jadavpur University, Kolkata. His Ph.D. thesis was on Application of Intelligent Techniques in Optimal Operation of Power System. Since then, he has been engaged in active research in different areas like automatic generation control, optimal operation of power system under conventional and non-conventional environment, control of renewable energy sources and micro-grid, image de-noising, video motion estimation, EEG-based emotion detection, and silent speech reading. He has more than 90 national and international publications in diverse fields. He has successfully completed four sponsored Research and Development projects. Further, he has been a Reviewer of number of international journals such as IEEE, IET, Elsevier, Taylor & Francis, and Springer.